J Solid State Electrochem (2008) 12:747–755
DOI 10.1007/s10008-007-0424-z

ORIGINAL PAPER

# Layer-by-layer assembly of $Ru^{3+}$ and $Si_8O_{20}^{8-}$ into electrochemically active silicate films

**Liza Rassaei · Mika Sillanpää · Elizabeth V. Milsom · Xiaohang Zhang · Frank Marken**

Received: 24 June 2007 / Revised: 30 August 2007 / Accepted: 31 August 2007 / Published online: 18 October 2007


**Abstract** A porous silicate is obtained from octa-anionic $Si_8O_{20}^{8-}$ cage-like poly-silicate (PS) and $Ru^{3+}$ cations in an ethanol-based layer-by-layer assembly process. Electrochemical experiments (voltammetry and impedance spectroscopy) confirm the formation of redox-active ruthenium centers in the form of hydrous ruthenium oxide throughout the film deposit. Oxidation of Ru(III) to Ru(IV) at a potential below 0.5 V vs saturated Calomel electrode (SCE) is reversible, but a potential positive of 0.5 V vs SCE is associated with an irreversible change in reactivity, which is characteristic for very small hydrous ruthenium oxide nanoparticles. Further voltammetric experiments are performed in aqueous phosphate buffer solutions, and the effects of number of layers, scan rate, and pH are investigated. Three aqueous redox systems are studied in contact with the PS–$Ru^{3+}$ films. The reduction of cationic methylene blue adsorbed onto the negative surface of the nanocomposite silicate is shown to occur, although most of the bound methylene blue appears to be electrochemically inactive either bound to silicate or buried into small pores. The PS–$Ru^{3+}$-catalyzed oxidations of hydroquinone and arsenite(III) are investigated. Scanning electron microscopy images show that a macroscopically uniform porous surface is formed after deposition of 50 layers of the PS–$Ru^{3+}$ nanocomposite. However, atomic force microscopy images demonstrate that in the initial deposition stages, irregular island growth occurs. The average rate of thickness increase for PS–$Ru^{3+}$ nanocomposite films is 6 nm per deposition cycle.

**Keywords** Layer-by-layer assembly · Ruthenium · Silsesquioxane · PSS · Silicate · ITO · Electrocatalysis · Voltammetry · Nanocomposite · Arsenite · Thin-film sensor

## Introduction

Extremely thin low-cost catalyst films are highly desirable in a wide variety of applications, and in recent years, layer-by-layer assembly processes have gained acceptance as simple and versatile techniques for fabricating ultrathin films on solid substrates [1–4] and for immobilizing metal oxide clusters into well-defined films approaching molecular thickness [5]. These two-component deposition processes offer a powerful method for altering physical properties of thin-film deposits at electrodes [6, 7] and a rapid and experimentally simple method to produce complex layered structures with precise control over the layer composition and thickness [8–11]. Moreover, wet layer-by-layer deposition has the advantage of low cost and high throughput of production in comparison to other techniques, e.g., requiring vacuum conditions for preparing nanostructures. The layer-by-layer deposition technique can be based for example on the alternating adsorption of oppositely charged poly-electrolytes onto a solid surface. The deposition occurs from solutions and is usually dominated by the electrostatic interaction between the polymeric or nanoparticulate components [12, 13]. However, this process may also be applied for films prepared from smaller molecular cationic and anionic building

L. Rassaei · M. Sillanpää
Laboratory of Applied Environmental Chemistry,
University of Kuopio,
Patteristonkatu 1,
50101 Mikkeli, Finland

E. V. Milsom · X. Zhang · F. Marken (✉)
Department of Chemistry, University of Bath,
Bath BA2 7AY, UK
e-mail: F.Marken@bath.ac.uk

blocks as shown for example for Prussian blue films [14, 15] or ferrocene derivatives [16]. In this report, we demonstrate facile silicate thin-film growth from molecular octa-anionic $Si_8O_{20}^{8-}$ poly-silicate (PS) anions.

Ruthenium oxide has long been recognized as an important electrode material in energy or charge storage [17], as an anode material [18], and as an efficient electrocatalyst in a large number of reactions of commercial and environmental importance [19, 20]. The relatively low surface area of unsupported ruthenium oxides restricts catalytic applications, and there have been considerable efforts to prepare highly porous supported ruthenium oxide electrodes. Excellent dispersion of ruthenium oxide catalysts has been reported on support materials like zeolite [21], $SiO_2$ [22, 23], $TiO_2$ [24], carbon [25], and carbon nanotubes [26].

Organic functionalized mesoporous silicas represented a new class of materials for the design of catalysts, in particular because of high surface area, controllable pore structures, and tailored pore surface chemistry, which allowed the binding of a large number of surface chemical moieties [27, 28]. The building blocks for many of these materials are silsesquioxanes, which derive from the octa-anionic PS cage structure shown in Fig. 1. In the present work, a simple method has been devised to form novel ultrathin silicate films from the octa-anionic PS and $Ru^{3+}$. The electrocatalytic behavior of hydrous ruthenium oxide embedded in the resulting silicate support on tin-doped indium oxide (ITO) electrode surfaces is investigated. The silicate-supported electrocatalyst is examined by electron and probe microscopies. Voltammetry is employed to explore the electrocatalyst performance in the reversible oxidation of hydroquinone and the irreversible oxidation of arsenite(III) in aqueous buffer media.

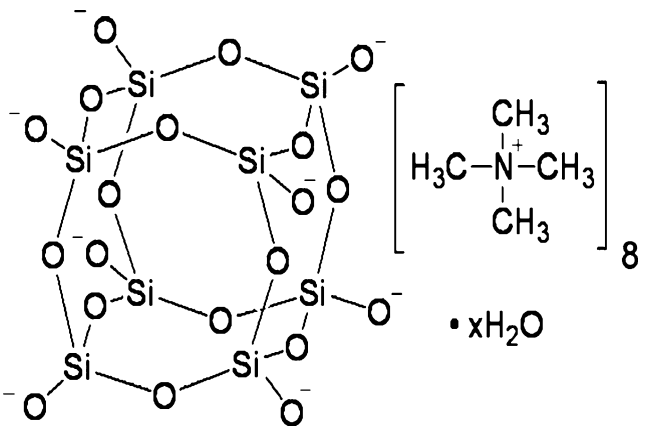


**Fig. 1** Schematic drawing of octakis(tetramethylammonium) pentacyclo-[9.5.1.13,9.15,15.17,13]-octasiloxane-1,3,5,7,9,11,13,15-octakis (yloxide) hydrate (PS)

## Experimental

### Chemical reagents

Chemical reagents such phosphoric acid (85 wt% solution in water American Chemical Society reagent), NaOH, KCl (all Aldrich), ethanol (Fisher Scientific), octakis (tetramethylammonium) pentacyclo-[9.5.1.13,9.15, 15.17,13]-octasiloxane-1,3,5,7,9,11,13,15-octakis(yloxide) hydrate (or poly-silsesquioxane silicate, PS, Aldrich), and ruthenium(III) chloride ($RuCl_3$, Ventron, Germany) were obtained commercially and used without further purification. All solutions were prepared using deionized and filtered water taken from an ELIX system (Millipore) with a resistivity of not less than 18 MΩ cm. Argon (Pure shield, BOC) was employed for deaeration of electrolyte solutions.

### Instrumentation

For voltammetric studies, a microAutolab III potentiostat system (EcoChemie, The Netherlands) was employed with a Pt gauze counter electrode and a saturated Calomel (SCE) reference electrode (Radiometer, Copenhagen). The working electrodes were made from ITO-coated glass (10× 0 mm, 15 Ω per square, Image Optics, Basildon, UK). The ITO electrodes were rinsed with ethanol and water, heat treated in a tube furnace (Elite Thermal Systems) for 1 h at 500 °C, and re-equilibrated to ambient conditions before use. Voltammograms were recorded in staircase mode (0.45 mV step potential), and impedance data were recorded over a frequency range of 50 kHz to 0.5 Hz with a fixed potential and an amplitude of 10 mV.

Scanning electron microscopy (SEM) images were obtained with a JEOL JSM6310 system, and the samples were gold sputter coated for 30 s before taking images. Atomic force microscopy (AFM) images were obtained with a Digital Instruments Nanoscope IIIa MultiMode Scanning Probe Microscope in the AFM contact mode. The temperature during experiments was 20±2 °C.

### Layer-by-layer formation of PS–$Ru^{3+}$ composite films

A layer-by-layer deposition strategy [29] was chosen to prepare thin-layer electrodes. A solution of $Si_8O_{20}^{8-}$ (or PS; 10 mM) and a solution of $RuCl_3$ (10 mM) both in ethanol were prepared separately. For deposition to occur, the ITO electrode was dipped first into the $RuCl_3$ solution for 20 s and then rinsed with ethanol and dried, and then it was dipped into PS solution for 20 s, rinsed with ethanol, and dried. This procedure is repeated to build up multilayer films. Very similar results were observed for $Ru^{3+}$-terminated and for PS-terminated films. Because of the volatility of ethanol

and the slow degradation (polymerisation) of PS solutions for each series of experiments, solutions were freshly prepared. Heat-treated film electrodes were prepared by placing the multilayer film electrode into a tube furnace at 500 °C for 30 min.

## Results and discussion

### Formation and electrochemical characterisation of mesoporous PS–$Ru^{3+}$ thin-film electrodes

The preparation of thin films via layer-by-layer deposition requires two reactive components (often cationic and anionic), which are deposited from two separate solutions in a dip-absorption process. There are many examples of this procedure being used for the assembly of colloidal particles and poly-electrolytes [30]. However, there are only a handful of examples (including Prussian blue films [13], some poly-oxometalates [31], metal cation bound nanoparticles [32], and metal complexes [33]) of this strategy being applied to smaller molecular systems. In this study, a silicate octa-anion is bound to a substrate with the help of $Ru^{3+}$ cations. The process is possible also with cations such as $Al^{3+}$ and $Fe^{3+}$, but it is most readily studied for the electrochemically active $Ru^{3+}$. Both reagents, $RuCl_3$ and the tetramethylammonium salt of PS, are soluble in absolute ethanol and a simple dip-coating process with an ITO electrode as substrate proved successful.

AFM was employed to image the progress of the deposition process and to obtain information about uniformity of the process. Figure 2a and b show images of a 10- and a 40-layer PS–$Ru^{3+}$ deposit. Initial stages of the film growth (not shown) clearly show island formation and nonuniform growth, but after ten and more deposition cycles, a steadily growing more uniform film is observed. Height measurements across scratch lines allow the growth per deposition cycle to be estimated as 6 nm in average (see Fig. 2c). SEM images obtained for the PS–$Ru^{3+}$ film show a uniformly porous film (see Fig. 2d).

Electrochemical measurements were conducted in aqueous 0.1 M phosphate buffer. Figure 3a shows cyclic voltammograms, which reveal a reversible surface-immobilized redox system centered at approx. 0.1 V vs SCE. With each deposition cycle, this response is increased, and a plot of the charge under the peak vs the number of deposition layers is shown in Fig. 3b.

The peak feature at 0.1 V vs SCE observed in voltammograms is relatively broad and very similar to a feature reported previously for hydrous ruthenium oxide nanoparticles [34]. From the charge under the peak (1.3 μC per layer per $cm^2$, see Fig. 3), it can be estimated that approximately only one electron is transferred for a film volume of 4×4×4 nm, and therefore, only a small fraction of the ruthenium present in the film (or only a fraction of the film) appears to be reacting. It seems most likely that during the deposition process (and exposure to moisture), restructuring occurs, and very small nanoparticles of hydrous $Ru_2O_3$ embedded into a silicate matrix are formed. Consistent with earlier studies [32], the observed voltam-

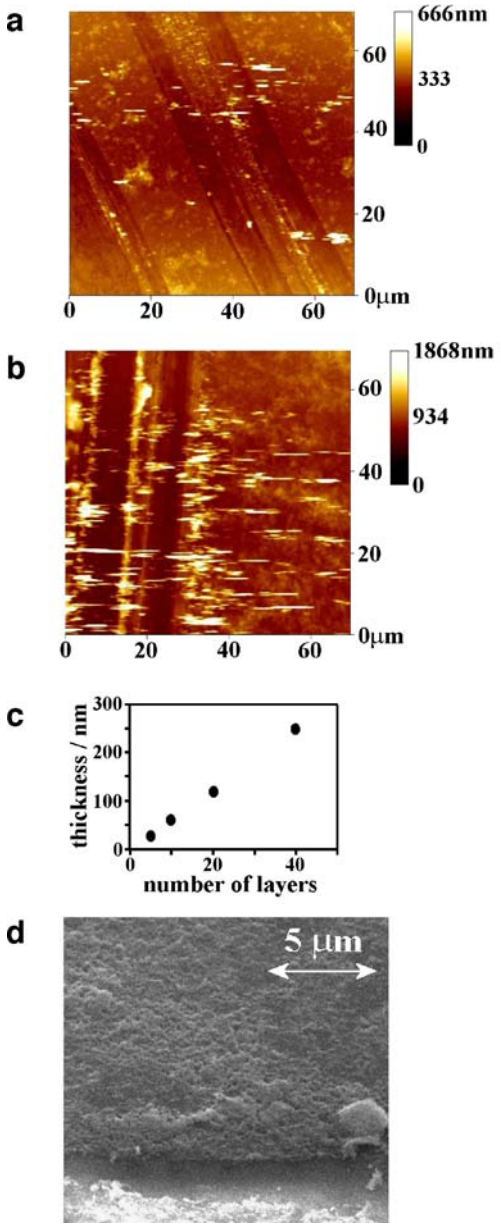


**Fig. 2** **a, b** AFM images of PS–$Ru^{3+}$ film deposits for a 10- and a 40-layer deposit. **c** Plot of the approximate thickness from AFM cross section analysis versus the number of deposition cycles. **d** SEM image of a 55-layer PS–$Ru^{3+}$ film on ITO. All samples were scratched with a scalpel before imaging to expose the substrate

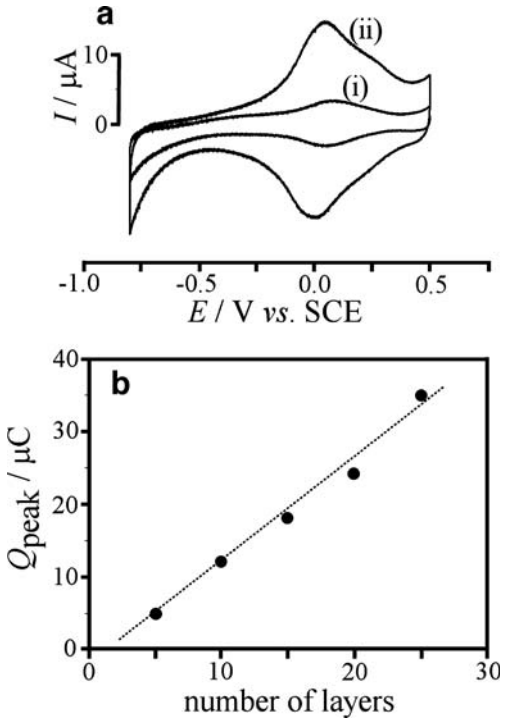


**Fig. 3** **a** Cyclic voltammograms (scan rate 0.1 V $s^{-1}$) for *i* 5 layers and *ii* 25 layers of PS–$Ru^{3+}$ film deposit on an ITO surface (area 1 $cm^2$) immersed in aqueous 0.1 M phosphate buffer at pH 7. **b** Plot of the charge under the cathodic current peak vs the number of PS–$Ru^{3+}$ layers

metric signal may be tentatively assigned to a Ru(IV/III) process at the surface of hydrous ruthenium oxide nanoparticles (Eq. 1).

$$\mathrm{Ru(III)(-OH)(surface)} \rightleftarrows \mathrm{Ru(IV)(=O)(surface)} + \mathrm{H^+(aq)} + \mathrm{e^-(ITO)} \quad (1)$$

Consistent with a surface-immobilized redox system, the voltammetric peak feature at 0.1 V vs SCE increases linearly with both the number of deposited layers and the scan rate. To obtain additional information, impedance measurements were undertaken at a fixed potential of 0.1 V vs SCE (see Fig. 4).

The process described by Eq. 1 is associated with a typical semicircle response (see Fig. 4). Increasing the number of layers of PS–$Ru^{3+}$ deposit is affecting mainly the charge transfer resistance R2 and not the resistance R1 (which is predominantly the resistance in the ITO electrode) or the capacitance (associated the interfacial capacitance of the ITO electrode). Data extracted by simulation of impedance data with the simple and approximate equivalent circuit shown in the inset (Fig. 4) are summarised in Table 1.

The increase in R2 as a function of the number of deposition layers appears approximately linear for a sufficiently high

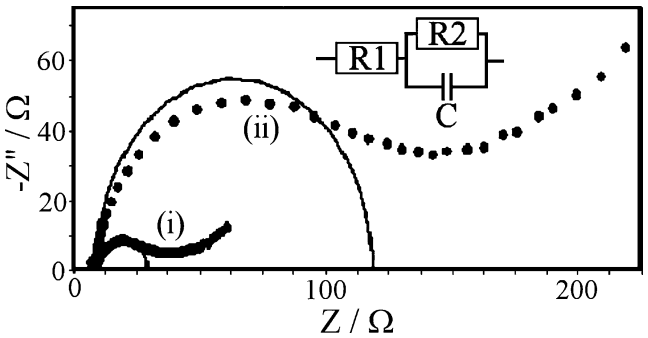


**Fig. 4** **a** Nyquist plots for the impedance data for *i* a one-layer PS–$Ru^{3+}$ film deposit and *ii* a 20-layer PS–$Ru^{3+}$ film deposit on ITO immersed in 0.1 M phosphate buffer pH 7. Data were recorded at a potential of 0.1 V vs SCE and over a frequency range of 50 kHz–0.5 Hz. *Solid lines* indicate simulation data (see Table 1) obtained with the equivalent circuit shown in the *inset*

number of layers, and this can be rationalized with the increase in the surface concentration of the Ru(III)(–OH) (surface) species affecting the apparent exchange current density. The relatively high value for R2 for the one-layer electrode could be a tell-tale sign for structural inhomogeneity and island growth (vide supra). The process observed at lower frequencies could be a slower follow-up redox step, e.g., a further Ru (III) reduction affecting less accessible redox centers within particles.

Next, the effect of the solution pH on the electrochemical response is investigated and demonstrated to be consistent with the process proposed in Eq. 1. Figure 5 shows cyclic voltammograms that shift systematically with pH by approximately 59 mV per pH unit.

These cyclic voltammograms reveal that the PS–$Ru^{3+}$ film is chemically stable in the pH range from at least 1 to 9. However, if the potential of the electrode is scanned into a more positive potential range, a new and chemically irreversible process is observed. Figure 6 shows a strong peak at 0.7 V vs SCE. After this oxidation process occurred, overall, the characteristics of the film have changed, and currents over the entire potential window are reduced.

A process very similar to this but with much sharper oxidation responses has been observed previously for hydrous ruthenium oxide nanoparticles [32]. The irrevers-

**Table 1** Impedance data obtained by fitting experimental data for PS–$Ru^{3+}$ film deposits on ITO immersed in 0.1 M phosphate buffer pH 7 with a fixed potential 0.1 V vs. SCE and a frequency range of 50 kHz – 0.5 Hz

| Electrode | R1 (Ω) | R2 (Ω) | *C* (μF) |
|---|---|---|---|
| 1 layer | 9.2 | 20 | 25 |
| 5 layer | 8.7 | 30 | 24 |
| 10 layer | 8.6 | 60 | 23 |
| 20 layer | 8.5 | 110 | 21 |

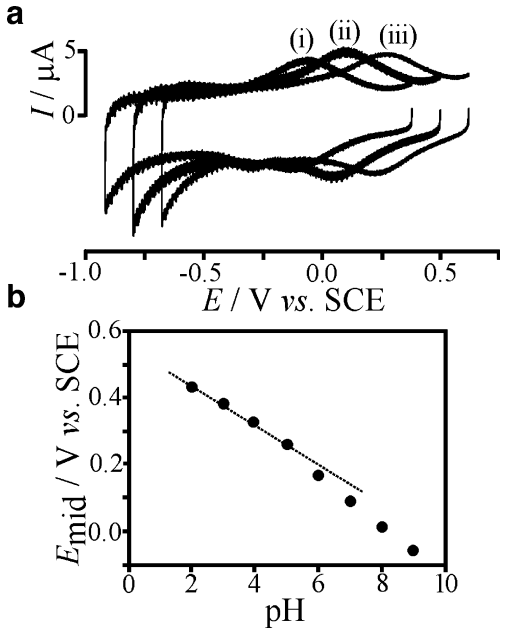


**Fig. 5** **a** Cyclic voltammograms (scan rate 0.1 V $s^{-1}$) for a ten-layer PS–$Ru^{3+}$ film deposit immersed in 0.1 M phosphate buffer at *i* pH 9, *ii* pH 7, and *iii* pH 5. **b** Plot of the midpoint potential vs pH (the *dotted line* corresponds to a 59-mV slope)

ible oxidation has been interpreted as (and is here tentatively assigned to) a Ru(IV/III) bulk process (Eq. 2).

$$\mathrm{Ru(III)(-OH)(bulk)} \rightarrow \mathrm{Ru(IV)(=O)(bulk)} + \mathrm{H^+(aq)} + \mathrm{e^-(ITO)} \quad (2)$$

Electrochemical processes at mesoporous PS–$Ru^{3+}$ thin-film electrodes in contact with the methylene blue redox system

Methylene blue (see structure in Fig. 7) is a positively charged and hydrophobic (surface active) molecule, which

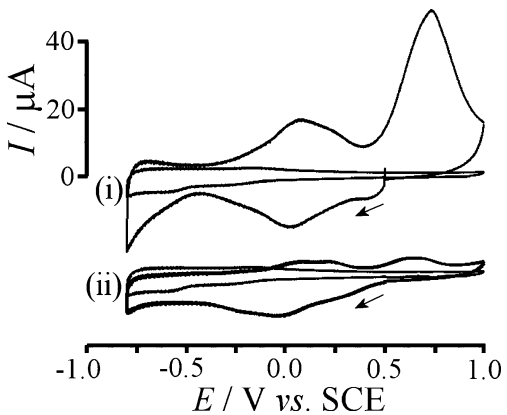


**Fig. 6** Cyclic voltammograms (scan rate 0.1 V $s^{-1}$) for a ten-layer PS–$Ru^{3+}$ film deposit (compared to a response obtained with a clean ITO electrode) immersed in 0.1 M phosphate buffer pH 7 for *i* the first potential cycle and *ii* the second potential cycle exploring the higher potential range

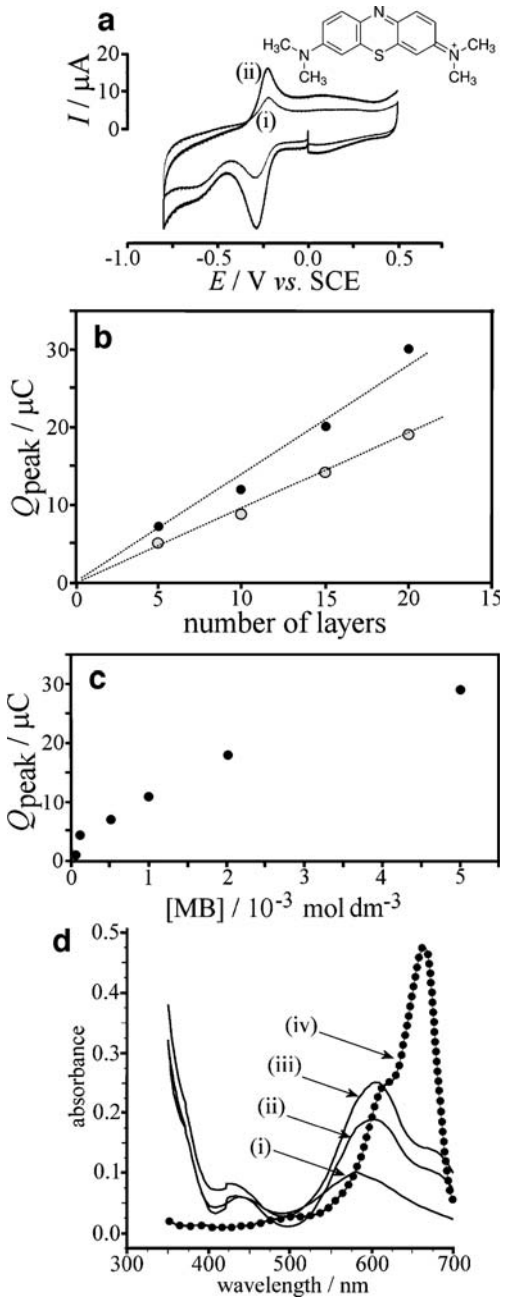


**Fig. 7** **a** Cyclic voltammograms (scan rate 0.1 V $s^{-1}$, area 1 $cm^2$) for *i* a five-layer PS–$Ru^{3+}$ film deposit and *ii* a ten-layer PS–$Ru^{3+}$ film deposit obtained in 0.1 M phosphate buffer pH 7 after 10-min immersion in a 1 mM methylene blue solution in 0.1 M phosphate buffer pH 7 and rinsing with water. **b** Plot of charge under the peak current vs the number of layers for a PS–$Ru^{3+}$ deposit before (*full circles*) and after (*empty circles*) bulk oxidation. **c** Plot of the charge under the peak observed for the reduction of methylene blue on a ten-layer PS–$Ru^{3+}$ electrode vs concentration of methylene blue in 0.1 M phosphate buffer pH 7 immersion solution. **d** UV/Vis data for PS–$Ru^{3+}$ films *i* one layer, *ii* five layers, and *iii* eight layers (after 10-min immersion in a 1 mM methylene blue solution in 0.1 M phosphate buffer pH 7 and rinsing with water) and *iv* a 8 μM methylene blue solution in 0.1 M phosphate buffer pH 7 in a 1-cm path length cuvette

is readily adsorbed onto the silica surface [35]. In this study, the two-electron reduction of methylene blue [36] is exploited to explore the reactivity of surface sites and to obtain an additional estimate of the surface area and porosity of the PS–$Ru^{3+}$ film deposits.

Immersion of the porous film electrode into a solution of 1 mM methylene blue in 0.1 M phosphate buffer (pH 7) allows methylene blue to be immobilized and adsorbed into the pores. The blue color of the dye adsorbed onto five- or ten-layer PS–$Ru^{3+}$ electrodes is clearly observed and therefore substantial. Rinsing, reimmersion into clean buffer solution, and scanning the potential of the electrode allows a new redox process to be observed at −0.25 V vs SCE (see Fig. 7a). This process is consistent with literature reports for the two-electron reduction of methylene blue [34]. This kind of experiment carried out at various methylene blue concentrations (see Fig. 7c) shows a weak dependence on the methylene blue concentration, and therefore, the charge under the reduction peak is not a well-defined measure of surface area. In fact, the adsorption of methylene blue onto silicas is likely to result in aggregates [37]. The analysis of the charge per deposition cycle suggests an apparently insignificant increase in surface area (approx. 10 μC for a ten-layer correspond to approx. 4% increase in area each deposition cycle [38, 39]), although a systematic change with each deposition cycle occurs (see Fig. 7b). The bulk oxidation of PS–$Ru^{3+}$ films also seems not to significantly affect the amount of electrochemically active methylene blue or the porosity (see Fig. 7b). However, no color change of the adsorbed methylene blue occurs during potential cycling, and therefore, most of the adsorbed dye appears to remain electrochemically inactive.

To obtain an estimate of adsorbed methylene blue, UV/Vis spectra were obtained. Figure 7d shows a typical solution-phase UV/Vis spectrum for 8 μM methylene blue in 0.1 M phosphate buffer pH 7 (curve iv) compared to spectra for a one-, a five- (curve ii), and an eight-layer PS–$Ru^{3+}$ film (curve iii). Adsorption of methylene blue onto silica surfaces is believed to result in aggregates with electronic properties different from solution-phase methylene blue, and this is reflected in the change in the shape of the absorption band (see Fig. 7d). Moreover, the increase in absorption appears nonlinear with film thickness probably because of aggregation and the additional opaqueness of the film. A very approximate estimate of the number of methylene blue adsorbed in the first PS–$Ru^{3+}$ layer (obtained at 610 nm and ignoring changes in oscillator strength) suggests a considerable increase in area for each deposition cycle (a roughness factor increase of 10 per deposition layer is calculated assuming an area of 120 $Å^2$ per molecule [36]) consistent with high porosity and many binding sites for methylene blue on the silicate surface. However, methylene blue at these binding sites appears electrochemically inaccessible.

## Electrochemical processes at mesoporous PS–$Ru^{3+}$ thin-film electrodes in contact with the hydroquionone–benzoquinone redox system

Hydrous ruthenium oxide is a well-known electrocatalyst material with applications such as insulin detection [40], analysis of dopamine and uric acid [41], or methanol oxidation [42]. To further explore the reactivity of the related PS–$Ru^{3+}$ films produced here, the hydroquionone–benzoquinone redox system was employed. The oxidation of hydroquinone follows a two electron–two proton pathway and is known to be exceptionally slow on clean ITO electrodes [43].

In initial exploratory experiments, it was observed that PS–$Ru^{3+}$ films even after only one-layer deposition exhibited considerable electrocatalytic activity for the oxidation of hydroquinone. Figure 8a shows the oxidation of 1 mM hydroquionone in 0.1 M phosphate buffer pH 7. Both the oxidation of hydroquinone and the reduction of benzoquionone are catalyzed by the PS–$Ru^{3+}$ film (see curve ii) when compared to bare ITO (see curve i). Next, the effect of the number of deposition layers on the oxidation process was investigated. An improvement is

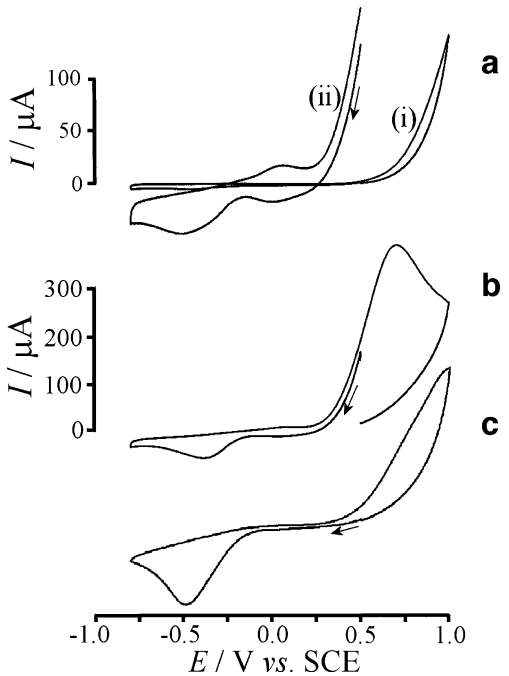


**Fig. 8** **a** Cyclic voltammograms (scan rate 0.1 V $s^{-1}$, area 1 $cm^2$) *i* for a clean ITO electrode and *ii* for a ten-layer PS–$Ru^{3+}$ film deposit on ITO immersed in 1 mM hydroquinone in 0.1 M phosphate buffer pH 7. **b**, **c** Cyclic voltammograms obtained over a wider potential range showing **b** the first scan for a ten-layer PS–$Ru^{3+}$ film deposit and **c** the second cycle (after bulk oxidation) immersed in 1 mM hydroquinone in 0.1 M phosphate buffer pH 7

observed for up to 10 layer deposits (not shown) but the effect of PS–$Ru^{3+}$ thickness is not pronounced.

It is interesting to explore the effect of the oxidation of the PS–$Ru^{3+}$ film at potential positive of 0.5 V vs SCE on the electrocatalysis process. Figure 8b and c show a multicycle voltammogram in which the anodic conversion of the PS–$Ru^{3+}$ film occurs in the first potential cycle (Fig. 8b). It can be seen that this is reducing the efficiency of the PS–$Ru^{3+}$ film in the second potential cycle (Fig. 8c) where the oxidation of hydroquinone is shifted to more positive potentials. Most effective in the transfer of electrons to hydroquinone appears to be the freshly deposited PS–$Ru^{3+}$ film.

## Electrochemical processes at mesoporous PS–$Ru^{3+}$ thin-film electrodes in contact with the arsenite(III) redox system

Next, the catalytic oxidation of arsenite(III) is considered. Arsenite(III) occurs naturally for example in drinking water wells [44] and has been determined most sensitively by electroanalysis at gold [45, 46] or platinum [47, 48] nanoparticle-decorated electrodes. In addition, metal complexes such as $Ru(bpy)_3^{2+}$ immobilized into metal oxide structures [49, 50] and metallo-dendrimer complex structures [51] have been shown to act as potent electrocatalysts, and $RuO_2$ is known to catalyze the ceric-driven oxidation of arsenite [52]. Therefore, it seemed possible that the PS–$Ru^{3+}$ film would allow the electrocatalytic oxidation of $AsO_3^{3-}$ to $AsO_4^{3-}$ in the presence of phosphate.

Initial exploratory voltammetric experiments suggested that no significant electrocatalytic current occurs at potential negative of 0.5 V vs SCE. However, when the potential is scanned positive of 0.5 V vs SCE, the onset of an anodic process is observed (see Fig. 9a). Increasing the thickness of the PS–$Ru^{3+}$ film did increase the observed current, and it was decided to explore the full potential range up to 1.5 V vs SCE in spite of the oxidation of the PS–$Ru^{3+}$ film. Figure 9b shows that the onset of a current response at 0.5 V vs SCE is followed by a broad current peak at

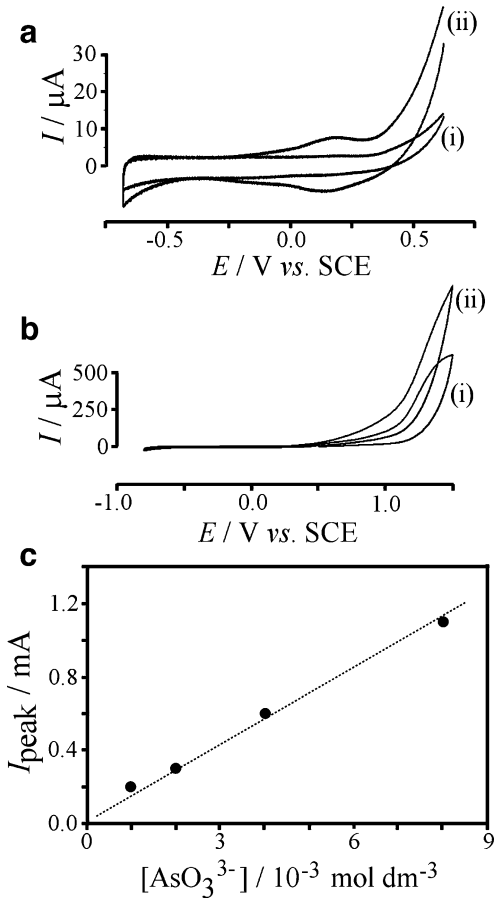


**Fig. 9** **a** Cyclic voltammograms (scan rate 0.1 V $s^{-1}$, area 1 $cm^2$) for *i* a one-layer PS–$Ru^{3+}$ film deposit and *ii* a 15-layer PS–$Ru^{3+}$ film deposit on ITO immersed in 1 mM $AsO_3^{3-}$ in 0.1 M phosphate buffer pH 5. **b** Cyclic voltammograms (scan rate 0.1 V $s^{-1}$) for a five-layer PS–$Ru^{3+}$ film deposit immersed in *i* 4 mM $AsO_3^{3-}$ and *ii* 8 Mm $AsO_3^{3-}$ in 0.1 M phosphate buffer pH 5. **c** Plot of peak current for the $AsO_3^{3-}$ oxidation vs the concentration of $AsO_3^{3-}$ in 0.1 M phosphate buffer pH 5

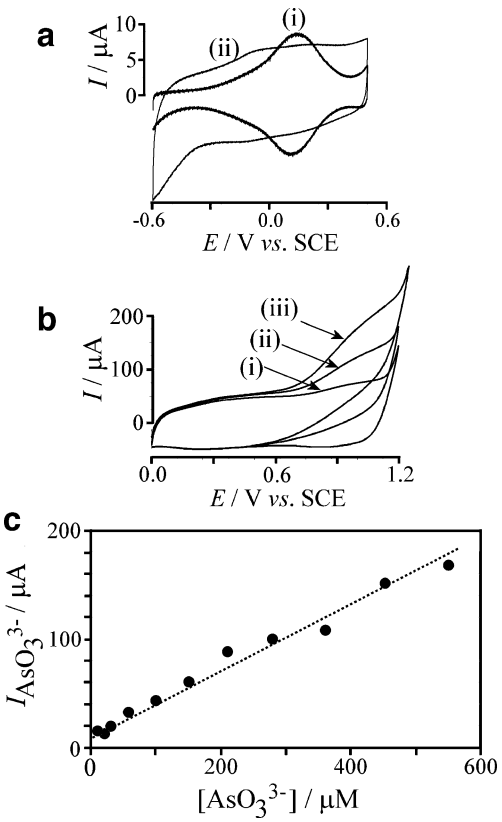


**Fig. 10** **a** Cyclic voltammograms (scan rate 0.1 V $s^{-1}$, area 1 $cm^2$) for *i* a five-layer PS–$Ru^{3+}$ film deposit and *ii* a heat-treated five-layer PS–$Ru^{3+}$ film deposit on ITO immersed in 0.1 M phosphate buffer pH 7. **b** Cyclic voltammograms (scan rate 0.01 V $s^{-1}$) for a heat-treated five-layer PS–$Ru^{3+}$ film electrode immersed in *i* 0.03 mM $AsO_3^{3-}$, *ii* 0.21 mM $AsO_3^{3-}$, and *iii* 0.55 mM $AsO_3^{3-}$ in 0.1 M phosphate buffer pH 2. **c** Plot of peak current for the $AsO_3^{3-}$ oxidation vs the concentration of $AsO_3^{3-}$ in 0.1 M phosphate buffer pH 2

approx. 1.3 V vs SCE, which is indeed approximately correlated to the concentration of arsenite(III) (see Fig. 9c). Unfortunately, this oxidation process is irreversible, and in a second and subsequent potential cycle, the electrode is completely inactive (not shown).

The observation of an electrocatalytic process for the arsenite oxidation at PS–$Ru^{3+}$ seemed promising and an indication that PS–$Ru^{3+}$ or similar further improved films could be a useful tool in arsenite electroanalysis. However, the need for a new electrode for each voltammetric scan is very inconvenient.

Annealing or heat treatment at 500 °C (see "Experimental") can be applied to stabilize the voltammetric response. Figure 10 shows voltammograms obtained with a five-layer PS–$Ru^{3+}$ film electrode after annealing. In this case, the electrode is stable even after applying very positive potentials. The sensitivity toward arsenite is further improved by going to phosphate buffer pH 2, and results for the detection of $AsO_3^{3-}$ down to 10 μM are shown in Fig. 10c.

During heat treatment, ruthenium oxide is known to undergo a structural change to $RuO_2$ [53], and this is believed to stabilize the film toward dissolution. The sensitivity toward arsenite is clearly improved and the behavior of the five-layer film deposit promising. Further improvements in sensitivity and efficiency will be possible for example by employing flow injection analysis, further optimizing the surface area and by further minimizing the amount of ruthenium used in the film formation.

## Summary

In this work, a novel nanocomposite material with ruthenium(III) incorporated into a $Si_8O_{20}^{8-}$ PS on ITO has been formed in a layer-by-layer process. This is the first demonstration of an octa-anionic silicate cage as a building block to form thin-film silicate structures, and it is likely that there are many other cationic building blocks or derivatives of $Si_8O_{20}^{8-}$ available to form a new family of thin-film silicate materials.

Exploratory voltammetric experiments demonstrate the reactivity of $Ru^{3+}$ as being similar to that observed previously for hydrous ruthenium oxide nanoparticles. From this observation, it is clear that the PS–$Ru^{3+}$ film structure is highly disordered and not based on a simple layer-by-layer architecture. A highly porous silicate structure is formed with anionic binding sites for methylene blue adsorption and electrocatalytic reactivity toward hydroquionone and arsenite(III) oxidation.

**Acknowledgment** The authors would like to thank the EU and TEKES, Finnish Funding Agency for Technology and Innovation for financial supports for this work.

## References

1. Decher G, Schlenoff J (2003) Multilayer thin films. Wiley-VCH, Weinheim
2. Farhat TR, Hammond PT (2006) Chem Mater 18:41
3. Park SY, Rubner MF, Mayes AM (2002) Langmuir 18:9600
4. Pastoriza-Santos I, Koktysh DS, Mamedov AA, Giersig M, Kotov NA, Liz- Marzán LM (2000) Langmuir 16:2731
5. Cheng L, Dong S (2000) J Electroanal Chem 481:168
6. McKenzie KJ, Marken F, Hyde M, Compton RG (2002) New J Chem 26:625
7. McKenzie KJ, Marken F, Oyama M, Gardner CE, Macpherson JV (2004) Electroanalysis 16:89
8. Escorcia A, Dhirani AA (2007) J Electroanal Chem 601:260
9. Kovtyukhova NI, Martin BR, Mbindyo JKN, Smith PA, Razavi B, Mayer TS, Mallouk TE (2001) J Phys Chem B 105:8762
10. Milsom EV, Perrott HR, Peter LM, Marken F (2005) Langmuir 21:9482
11. Amiri M, Shahrokhian S, Marken F (2007) Electroanalysis 19:1032
12. Decher G (1997) Photonic and Optoelectronic Polymers ACS Symp Ser 672:445
13. Bonné MJ, Milsom EV, Helton M, Thielemans W, Wilkins S, Marken F (2007) Electrochem Commun 9:1985
14. Millward RC, Madden CE, Sutherland I, Mortimer RJ, Fletcher S, Marken F (2001) Chem Commun 19:1994
15. Jin WQ, Toutianoush A, Pyrasch M, Schnepf J, Gottschalk H, Rammensee W, Tieke B (2003) J Phys Chem B 107:12062
16. Asaftei S, Walder L (2004) Electrochim Acta 49:4679
17. Song RY, Park JH, Sivakkumar SR, Kim SH, Ko JM, Park DY, Jo SM, Kim DY (2007) J Power Sources 166:297
18. Cornell A, Hakansson B, Lindbergh G (2003) Electrochim Acta 48:473
19. Fachinotti E, Guerrini E, Tavares AC, Trasatti S (2007) J Electroanal Chem 600:103
20. Jirkovsky J, Makarova M, Krtil P (2006) Electrochem Commun 8:1417
21. Dutta PK, Vaidyalingam AS (2003) Micropor Mesopor Mater 62:107
22. Liu H, Iglesia E (2005) J Phys Chem B 109:2155
23. Armelao L, Barreca D, Moraru B (2003) J Non-Cryst Solids 316:364
24. Bavykin DV, Lapkin AA, Plucinski PK, Friedrich JM, Walsh FC (2005) J Catal 235:10
25. Mazurek M, Benker N, Roth C, Fuess H (2006) Fuel Cells 6:208
26. Cao L, Scheiba F, Roth C, Schweiger F, Cremers C, Stimming U, Fuess H, Chen LQ, Zhu WT, Qiu XP (2006) Angew Chem 45:5315
27. Kuroki M, Asefa T, Whitnal W, Kruk M, Yoshina-Ishii C, Jaroniec M, Ozin GA (2002) J Am Chem Soc 124:13886
28. Liu PT, Chang TC, Hsu KC, Tseng TY, Chen LM, Wang CJ, Sze SM (2002) Thin Solid Films 414:1
29. McKenzie KJ, Marken F (2003) Langmuir 19:4327
30. Stott SJ, Mortimer RJ, McKenzie KJ, Marken F (2005) Analyst 130:358
31. Wang L, Li J, Wang EB, Xu L, Peng J, Li Z (2004) Mater Lett 58:2027
32. Leopold MC, Donkers RL, Georganopoulou D, Fisher M, Zamborini FP, Murray RW (2004) Faraday Disc 125:63
33. Ma HY, Dong T, Wang FP, Zhang W, Zhou BB (2006) Electrochim Acta 51:4965
34. McKenzie KJ, Marken F (2002) Electrochem Solid State Lett 5:E47
35. Wang SB, Li HT (2006) Micropor Mesopor Mater 97:21
36. Piccardi G, Pergola F, Foresti ML, Guidelli R (1977) J Electroanal Chem 84:235

37. Avena MJ, Valenti LE, Pfaffen V, De Pauli CP (2001) Clays Clay Miner 49:168
38. Brina R, De Battisti A (1987) J Chem Educ 64:175
39. Giles CH, D'Silva AP (1969) Trans Faraday Soc 65:1943
40. Wang J, Tangkuaram T, Loyprasert S, Vazquez-Alvarez T, Veerasai W, Kanatharana P, Thavarungkul P (2007) Anal Chim Acta 581:1
41. Shakkthivel P, Chen SM (2007) Biosens Bioelectr 22:1680
42. Villullas HM, Mattos-Costa FI, Nascente PAP, Bulhoes LOS (2006) Chem Mater 18:5563
43. Stott SJ, Mortimer RJ, Dann SE, Oyama M, Marken F (2006) Phys Chem Chem Phys 8:5437
44. Cavicchioli A, La-Scalea MA, Gutz IGR (2004) Electroanalysis 16:697
45. Dai XA, Compton RG (2006) Anal Sci 22:567
46. Hignett G, Wadhawan JD, Lawrence NS, Hung DQ, Prado C, Marken F, Compton RG (2004) Electroanalysis 16:897
47. Ca DV, Sun LS, Cox JA (2006) Electrochim Acta 51:2188
48. Hrapovic S, Liu YL, Luong JHT (2007) Anal Chem 79:500
49. Wang XL, Zhang Q, Han ZB, Wang EB, Guo YQ, Hu CW (2004) J Electroanal Chem 563:221
50. Wang XL, Han ZB, Wang EB, Zhang H, Hu CW (2003) Electroanalysis 15:1460
51. Cheng L, Cox JA (2002) Chem Mater 14:6
52. Gajic-Krstajic LM, Trisovic TL, Krstajic NV (2004) Corr Sci 46:65
53. Ma HC, Liu CP, Liao JH, Su Y, Xue XZ, Xing W (2006) J Mol Cat A Chem 247:7